Arabian Journal of Chemistry (2020) 13, 7453–7458

King Saud University

Arabian Journal of Chemistry

www.ksu.edu.sa
www.sciencedirect.com

ORIGINAL ARTICLE

AC conductivity, structural, and dielectric properties of zinc supported on titanium dioxide: Facile synthesis and DFT calculation

Mohammed A.H. Khalafalla [a], **Ali H. Bashal** [b,*]

[a] *Department of Physics, Faculty of Science, Taibah University, Yanbu 46423, Saudi Arabia*
[b] *Department of Chemistry, Faculty of Science, Taibah University, Yanbu 46423, Saudi Arabia*

Received 11 May 2020; accepted 18 August 2020
Available online 27 August 2020

KEYWORDS

Zn/TiO_2;
Dielectric constant;
Ac conductivity;
First Principle Calculation;
Dielectric loss

Abstract We present a simple and systematic synthesis method of Zn doped TiO_2 (Zn/TiO_2) that is usually prepared with sophisticated preparation procedures. Zn/TiO_2 have been synthesized following a facile and efficient incipient wet impregnation method. The resulting Zn/TiO_2 has been characterized by X-ray diffraction, scanning electron microscopy, and energy-dispersive X-ray spectroscopy, which revealed the successful formation of the anatase phase and traces of the rutile phase. The existence of the rutile phase in smaller proportion was a clear sign of the Zn doping induced anatase-to-rutile phase transition. Sensible enhancement in the dielectric constant due to Zn addition has also been observed from experiment and approximate first-principle calculation. Thus, our results have significant impact on TiO_2 based semiconductor technology.

1. Introduction

Semiconductors have been broadly investigated in lots of applications along with digital, environmental, and energy programs (Tripathy and Pattanaik, 2016). This has drawn significant attention towards the development of these materials in order to enhance their physical characteristics. For example, owing to its versatile applications and cost effectiveness, titanium oxide (TiO_2) has become one of the mostly investigated semiconductor (Haider and R. H. AL–Anbari, G. R. Kadhim, and C. T. Salame, , 2017). The main crystal structures of TiO_2 are known as the rutile (tetragonal), anatase (tetragonal), and brookite (orthorhombic) (Sen et al., 2005). Moreover, among the various semiconductor materials used, TiO_2 has been used as a valuable photocatalyst (Chávez et al., 2020) and photoanode of sensitized solar cell (Deng et al., 2019) due to its attractive properties such as low toxicity, low price, oxidative strength, and low biological and chemical activity (Foulady-Dehaghi and Behpour, 2020). The challenges in using TiO_2 for photovoltaic processes are the need for an expensive and unsafe ultraviolet source, owing to the large band gap of TiO_2. Hence, the use of titanium oxide under visible sunlight meets strict restrictions. For example, when using TiO_2 in its pure form of impurities, a lot of light energy is

* Corresponding author.
E-mail address: abishil@taibahu.edu.sa (A.H. Bashal).
Peer review under responsibility of King Saud University.

ELSEVIER Production and hosting by Elsevier

https://doi.org/10.1016/j.arabjc.2020.08.021
1878-5352

needed to generate a very fast electron-hole pair, so the photocatalytic activity is reduced under visible light with low energy (Ahmadi et al., 2014). TiO_2 properties can be altered in the presence of impurities and dopants. The electrical and optical characteristics of TiO_2 can be promoted if doped with Sn and Zr (Cao et al., 2004); (Yu et al., 1998). Doping TiO_2 with metals can cause interesting phase transformation, for instance, from anatase to rutile, hence, improving the TiO_2 photocatalytic activity (Gaur, 2019); (Kalantari et al., 2017). Reports have shown improved TiO_2 photocatalytic activity associated with the coexisting anatase and rutile phases e.g. (Bickley et al., 1991); Ag (Chao et al., 2003); and Sn (Mahanty et al., 2004). Metals ions promote this transformation however, some other semi-metal ion such as Si has been found to hinder the structural transition between the anatase and rutile phases (Okada et al., 2001). Therefore, finding modified metal which can improve TiO_2 physical properties such as structural and dielectric properties and to promote its phase transformation is challenging. Several research groups have been attracted towards using Zn as a dopant for improving the photovoltage properties of TiO_2 (Zhu et al., 2010); (Yu et al., 2015); (Jing et al., 2006). However, these studies followed complex procedure for chemically preparing the material, thus, compromising the potential applications of this material. TiO_2 nanomaterials mixed with traces of (i.e. doped) zinc have several important optical applications for science and technology as well as its activity as a strong antibacterial material (Ye et al., 2020) so it is imperative to find a procedure for their easy, environmentally friendly and more efficient manufacturing.

TiO_2 doped with zinc has distinct chemical and physical properties since Zn-doping in TiO_2 gives an n-type dopant that helps in the transport of electrons. The doping process also helps control the light band gap of this material. TiO_2 doped with zinc was widely imposed on photocatalysis, leading to an enhancement in photoconduction compared to undoped TiO2 (Yu and Yu, Jul. 2008).

In this study, we prepared Zn/TiO_2 by simple incipient wet impregnation. The surface morphology, crystal structure, the grain growth of doped sample was investigated by EDS (X-ray energy-dispersive spectroscopy), XRD (X-ray diffraction), and scanning electron micrographs (SEM). We have also investigated the effect of introducing Zn^{2+} ions to TiO_2 on the dielectric properties, ac conductivity, and phase transformation of TiO_2. To the best of our knowledge, investigations about facile synthesis of Zn/TiO_2 and systematic dielectric and first-principle investigation of this material, are lacking.

2. Experimental

2.1. Materials

For the synthesis of metal oxide nanoparticles, zinc chloride (99.999% trace metals basis), and titanium oxide (≥99% trace metals basis), which were obtained from Sigma-Aldrich (USA). All aqueous solutions in the synthesis were prepared with deionized water and it was carried out by simple incipient wet impregnation. All chemicals were used without further purification beyond the provider's purification level.

2.2. Sample preparation

Zn/TiO_2 was prepared by the incipient wet impregnation method following the procedure described earlier (Bashal et al., 2020). TiO_2 (undoped) was dispersed in water under continuous stirring for 30 min. 5 wt% of $ZnCl_2$)(i.e. 0.014 g of Zn (~65 g/mol) in ZnCl2 (~136 g/mol) has been added to 1 g of TiO_2)(was dissolved in 3 ml of deionized water. The prepared solution was added dropwise to the stirred TiO_2 solution and then the mixture was left overnight at room temperature to dry in the oven at 120 °C. The obtained sample with a Zn loading amount of 5 wt% was marked as Zn/TiO_2.

In preparation for the electrical and various characterization, the samples were grounded utilizing a pestle and mortar to form fine powder. Otherwise, large particles would hinder the formation of smooth pellets. Then an amount of 0.30 g of the sample was compressed in a hydraulic die-set ket where the pellet was formed.

2.3. Sample characterization

Our samples were characterized with XRD to investigate their phase structures. The X-ray was from a Cu target with Kα radiation of λ = 0.15418 nm wavelength that was produced at 30 mA and 40 kV power supply. The surface morphology of the samples was investigated with the JEOL JSM-IT300 SEM instrument (https://www.jeol.co.jp/en/) that was supplemented with EDS (Electron-dispersive X-ray spectroscopy) module designed for the analysis of the surface elements. The measurements of the dielectric properties were performed using the Solareton Analytic impedance analyzer with an AC amplitude = 300 mV and 0.1 – 300 kHz frequency range at various temperatures

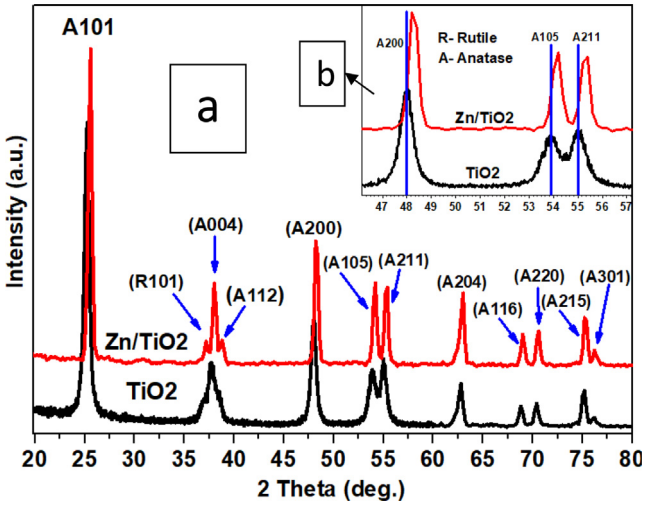

Fig. 1 a and b. XRD patterns of undoped TiO_2 and Zn/TiO_2.

3. Results and discussion

3.1. Characterisation of Zn/TiO_2

3.1.1. XRD

Fig. 1 illustrates the XRD spectrum for pure TiO_2 and Zn doped TiO_2 (Zn/TiO_2). The peaks associated with the rutile and anatase phases were identified and designated as 'R' and 'A', respectively. The quantities next to 'R' and 'A' in the curved parenthesis represented the corresponding miller planes of diffraction.

Several diffraction peaks were detected for undoped TiO_2 at $2\theta^o$ = 25.3°, 37.69°, 48.03°, 53.83°, 55.01°, 62.8°, 68.8°, 70.4°, 75.2°, and 76°, which could be assigned to the A101, A004, A200, A105, A211, A204, A116, A220, A215, and A301 diffraction planes. These planes are pertinent with the tetragonal phase for the pure anatase phase as reported by Wang et al (Wang et al., 2015). However, after Zn doping TiO_2, two diffraction peaks appeared at 2θ = 37.2° and 38.6° which can be assigned to (R101) and (A112) for rutile phase and anatase phase respectively. The diffraction peak at 2θ = 37.2° demonstrated the occurrence of tetragonal phase rutile TiO_2 in Zn doped TiO_2 sample. These data strongly suggest that the phase transition between the anatase and rutile was stimulated by the Zn doping. No diffraction peaks were observed for Zn which could be contributed to the low percentage of a prepared sample. Or the Zn particles are highly dispersed and too small to be detected by XRD. Furthermore, with the insertion the Zn^{2+} into TiO_2 matrix the diffraction peaks for Zn doped TiO_2 becomes more intense which indicate well crystalline nature of the prepared (Zn/TiO_2) (Mofokeng et al., 2017). The XRD peaks show a significant and noticeable shift towards high diffraction angle for Zn doped TiO_2 compared with undoped TiO_2. There are three TiO_2 anatase peaks, (A200), (A104), and (211) where this shift clearly noticed in Fig. 1(b). The shift is attributed to the enlargement of the TiO_2 structure (Diener, 2009). Because Zn^{2+} can diffuse into the titanate layer, it can dissolute in the lattice and replace Ti^{4+} (Nian et al., 2006). However, since Zn^{2+} (74×10^{-12}m = 74 pm) is larger than Ti^{4+} (60×10^{-12}m = 60 pm) (Xu et al., 2006), the substitution of Zn^{2+} for Ti^{4+} leads to TiO_2 lattice expansion. Therefore, the Zn doped TiO_2 is expected to take the alloy form $Zn_xTi_{1-x}O_2$ where the composition × determine the occupancy of the Ti lattice site by the Zn dopant (Wang and Teng, 2009). The structure of our samples is expected to be composed of crystallites. To estimate the size of the crystallite we employ Scherrer's equation. The crystallite size decreased from 19.57 nm (TiO_2) to 18.23 nm for Zn/TiO_2, indicating that Zn doping has induced the crystallite shrinkage.

3.1.2. SEM/EDS analysis

Fig. 2 shows the SEM images for the TiO_2 and the Zn/TiO_2. The SEM reveals pronounced difference between the microstructures for the undoped and doped sample. The granular structure for the undoped TiO_2 is smaller in average that for the doped one.

Compared with the doped TiO_2, the Zn/TiO_2 has a totally different morphology. For instance, the small particles in Zn/TiO_2 coalesce to form semispherical structures or grains as is evident from Fig. 2b. Furthermore, inspecting the SEM carefully may reveal the formation of small black holes or cavities in the Zn/TiO_2 microstructures that are reminiscent of the formation of similar holes associated with the order–disorder transition in TiO_2 as reported by S. A. El All (El All and El-Shobaky, 2009).

Fig. 3(a) shows the EDS elemental analysis performed in area shown by the SEM in Fig. 3(b) for Zn/TiO_2 sample.

The energetic position of Zn suggests that it is highly spread into TiO_2. The plot of the chemical composition in Fig. 3(b) shows intense X-ray peaks for Ti and O, which are the main elements in Zn doped TiO_2. Here, the proportions of Ti and O may reflect the average stoichiometry of 1:2. Additionally, the EDS peak intensity and percentage for Zn are consistent with relative weight percentage of Zn in TiO_2, indicating TiO_2 doping with Zn. To further support the data in Fig. 3, Transmission Electron Micrographs (TEM) for our samples will be provided in future works.

3.2. AC conductivity

The electrical conductivity, (σ) of TiO_2, and Zn/TiO_2 as a function of frequency are shown in Fig. 4. The values of ac conductivity can be given by $\sigma_{ac}(\omega) = \omega\varepsilon_o\varepsilon'' = B\omega^s$, where B is a pre-exponential factor, and s is the universal exponent, which determines the degree of interaction between mobile and lattices. Fig. 4 shows that the magnitude of the ac conductivity is almost invariant at low frequencies and monotonically increases above ~ 200 Hz which confirms the semiconductor nature of the Zn/TiO_2 and power law behavior. Similar behavior has been observed in Co doped TiO_2 as demonstrated by Okutan et al (Okutan et al., 2005). The effect of interface defects may be significant at low temperature, affecting the electrical properties at low 25 °C temperature.

The increase of σ with increasing the frequency may be due to the exchange of charges between the metal ions and dopant ions located at grain boundaries. In addition, the value of electrical conductivity for Zn doped TiO_2 is higher than that of undoped TiO_2, this may be the dopant atoms perfectly replace the Ti^{3+} site in the crystal lattice of TiO_2. Another possibility might be due to the holes (cavities) which present in Zn/TiO_2 as was observed in SEM results. Thus, the effective enhancement in the electrical conductivity in Zn/TiO_2 may be attributed to the stimulation of charge carrier diffusion by these holes (Tsai and Cheng, 1997). Fig. 4 also shows the thermally activated conductivity for Zn doped TiO_2.

3.3. Dielectric properties

Fig. 5(a) and (b) are, respectively, the dielectric constant (ε') for pure TiO_2 and Zn-TiO_2 as a function of the frequency (f) with the temperature as a parameter. ε' sharply increased as f reduces within the low frequency range, suggesting polarization and space charge formation at the sample-electrode interface (MacDonald, 1973). Since this is a relatively large area interface it has a large capacitance and hence a relatively large time constant for the polarization process of charges within the interface caused by the AC signal. Thus, those charges cannot follow the electric field oscillation at higher frequencies where processes with smaller

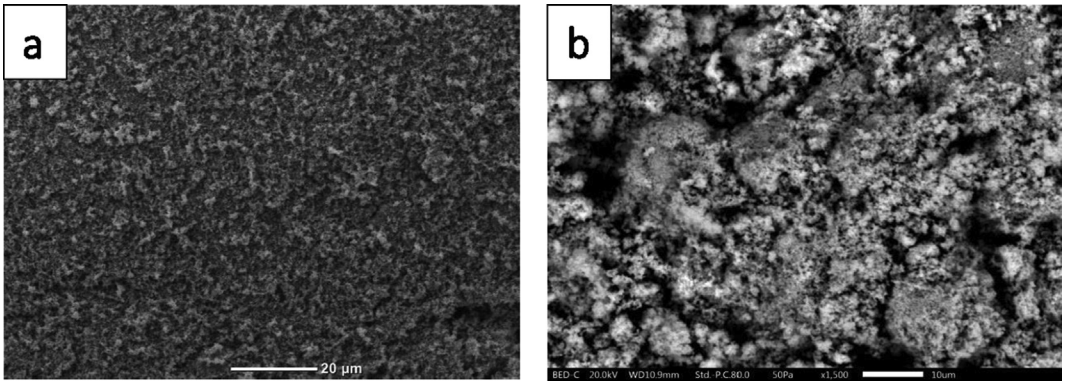

Fig. 2 SEM images of undoped TiO_2 (A), Zn/TiO_2 (b).

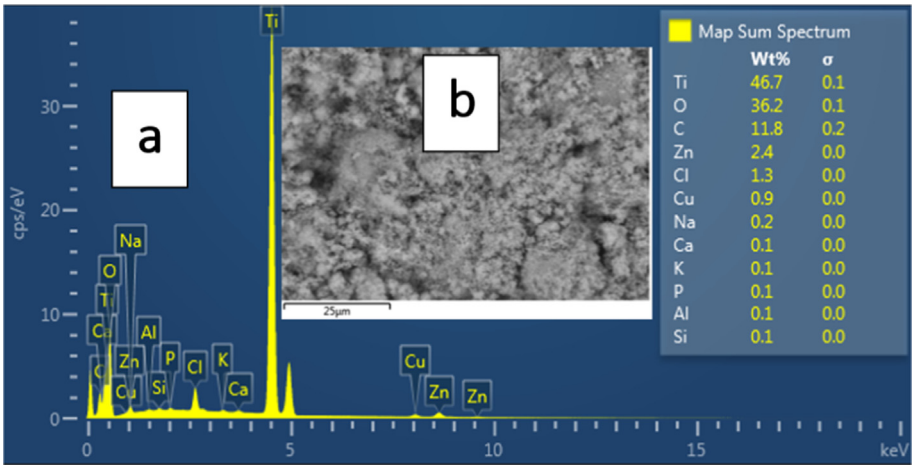

Fig. 3 The EDX results for Zn/TiO_2.

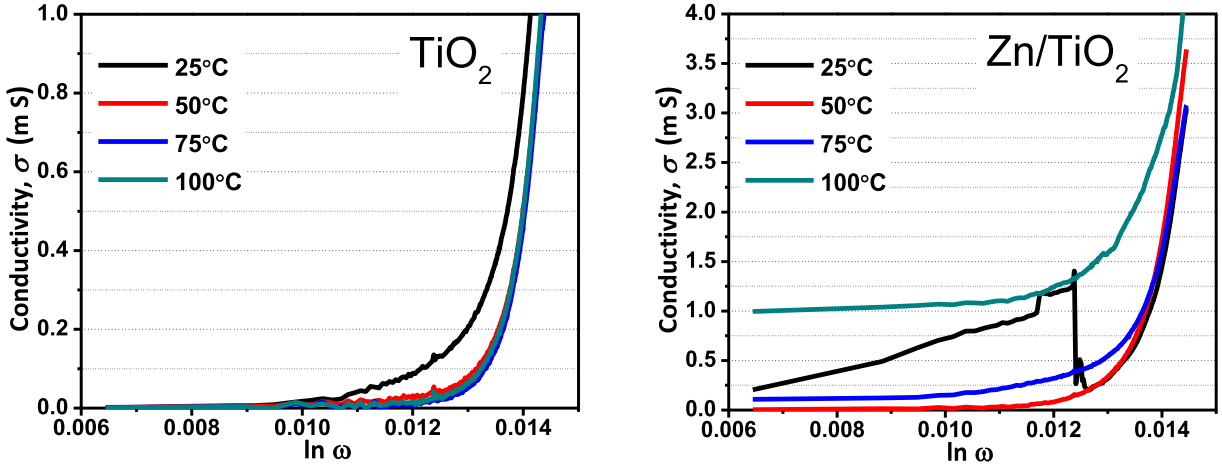

Fig. 4 Frequency dependence of σ_{ac} conductivity for 2 samples at different temperature.

time constants would emerge. The above-mentioned overall behavior is common for both TiO_2 and Zn-TiO_2, however, the effect of adding Zn to TiO_2 is to enhance the dielectric constant specifically at low frequencies. This may be due to the Zn induced increase of the free ions or charge carries in the material.

3.4. First-principle calculations

We have performed first-principle calculations of the optical-dielectric-constant for TiO_2 and 10%Zn-TiO_2 (Fig. 6) in order to roughly and qualitatively compare them with our experimental electrical dielectric-constant.

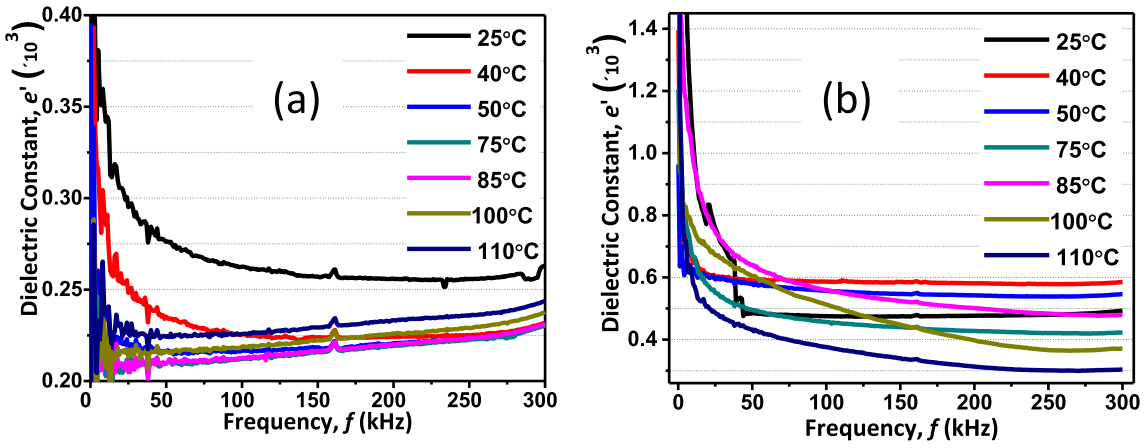

Fig. 5 (a) The dependence of the dielectric constant on the frequency at different temperatures for pure TiO_2. (b) dependence of the dielectric constant on the frequency at different temperatures for Zn-TiO_2.

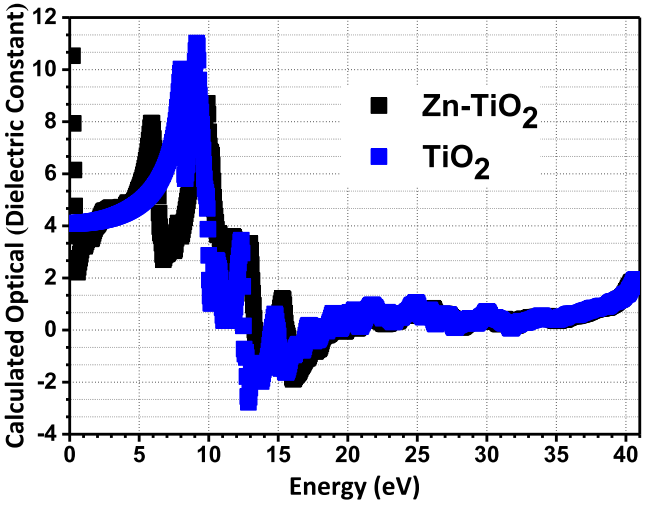

Fig. 6 The calculated (from first principle) optical dielectric constant versus the photonic energy for TiO_2 and 10% Zn-TiO_2.

We used ELK LAPW software (http://elk.sourceforge.net), utilizing the Random Phase Approximation (Chen et al., 2017). The results show that the effect of Zn is to slightly vary the characteristics specifically in the low frequency region (i.e low energy region, since the photon energy is directly proportional to the frequency). Busani et al (Busani and Devine, 2005) (has performed experimental measurement of the properties of TiO_2, where the dielectric constant extracted from the Polarizability has approximately the same order of magnitude as ours (Fig. 6) at low energy (i.e low frequency).

This behavior qualitatively and roughly agrees with the experimental results in Fig. 5 where we observe that the variation in the characteristics due to Zn addition is more pronounced in the low frequency region. It is worth pointing out that the first principle calculations were done for the ground state configuration associated with 0 K temperature. However, these calculations can still convey information related to semiconductors and insulators at temperatures close to the room temperature.

4. Conclusion

We managed to synthesize the Zn doped TiO_2 (Zn/TiO_2) using a facile and efficient incipient wet impregnation method. The resulting Zn/TiO_2 has been characterized by X-ray diffraction, scanning electron microscopy, and energy-dispersive X-ray spectroscopy. The X-ray diffraction peaks revealed the successful formation of the anatase phase and traces of the rutile phase as evident from the positions of the X-ray peaks. The formation of the rutile was associated with the Zn doping induced anatase-to-rutile phase transition. Investigation of the enhancement of the photocatalytic behavior of Zn/TiO_2 will be considered in future work. Comparison between the conductivity in bare and doped TiO_2 revealed a conductivity improvement in the doped samples due to improved charge carrier diffusion through microstructures induced by the doping. Sensible enhancement in the dielectric constant due to Zn addition has also been observed from experiment and approximate first-principle calculation. Therefore, our results have significant impact on TiO_2 based semiconductor technology.

References

Ahmadi, N., Nemati, A., Solati-Hashjin, M., 2014. Synthesis and characterization of co-doped TiO2 thin films on glass-ceramic. Mater. Sci. Semicond. Process. 26, 41–48.

Bashal, A.H., Saad, M.H., Khalafalla, M.A., 2020. The effect of Nickel percentage on the dielectric properties of Bentonite. J. Taibah Univ. Sci. 14 (1), 496–499.

Bickley, R.I., Gonzalez-Carreno, T., Lees, J.S., Palmisano, L., Tilley, R.J., 1991. A structural investigation of titanium dioxide photocatalysts. J. Solid State Chem. 92 (1), 178–190.

Busani, T., Devine, R., 2005. Dielectric and infrared properties of TiO2 films containing anatase and rutile. Semicond. Sci. Technol. 20 (8), 870.

Cao, Y., Yang, W., Zhang, W., Liu, G., Yue, P., 2004. Improved photocatalytic activity of Sn 4+ doped TiO 2 nanoparticulate films prepared by plasma-enhanced chemical vapor deposition. New J. Chem. 28 (2), 218–222.

Chao, H., Yun, Y., Xingfang, H., Larbot, A., 2003. Effect of silver doping on the phase transformation and grain growth of sol-gel titania powder. J. Eur. Ceram. Soc. 23 (9), 1457–1464.

Chávez, A.M., Solís, R.R., Beltrán, F.J., 2020. Magnetic graphene TiO2-based photocatalyst for the removal of pollutants of emerging concern in water by simulated sunlight aided photocatalytic ozonation. Appl. Catal. B 262, 118275.

Chen, G.P., Voora, V.K., Agee, M.M., Balasubramani, S.G., Furche, F., 2017. Random-phase approximation methods. Annu. Rev. Phys. Chem. 68, 421–445.

Deng, J., Wang, M., Fang, J., Song, X., Yang, Z., Yuan, Z., 2019. Synthesis of Zn-doped TiO2 nano-particles using metal Ti and Zn as raw materials and application in quantum dot sensitized solar cells. J. Alloy. Compd. 791, 371–379.

S. Diener, "Ageing behaviour of steel slags in landfill liners," 2009.

El All, S.A., El-Shobaky, G.A., 2009. Structural and electrical properties of γ-irradiated TiO2/Al2O3 composite prepared by sol–gel method. J. Alloy. Compd. 479 (1–2), 91–96.

Foulady-Dehaghi, R., Behpour, M., 2020. Visible and solar photodegradation of textile wastewater by multiple doped TiO2/Zn nanostructured thin films in fixed bed photoreactor mode. Inorg. Chem. Commun. 107946

Gaur, L.K. et al, 2019. Laser induced phase transformation influenced by Co doping in TiO2 nanoparticles. J. Alloy. Compd. 780, 25–34.

Haider, A.J., AL–Anbari, R.H., Kadhim, G.R., Salame, C.T., 2017. Exploring potential environmental applications of TiO2 nanoparticles. Energy Procedia 119, 332–345.

Jing, L., Xin, B., Yuan, F., Xue, L., Wang, B., Fu, H., 2006. Effects of surface oxygen vacancies on photophysical and photochemical processes of Zn-doped TiO2 nanoparticles and their relationships. J. Phys. Chem. B 110 (36), 17860–17865.

Kalantari, K., Kalbasi, M., Sohrabi, M., Royaee, S.J., 2017. Enhancing the photocatalytic oxidation of dibenzothiophene using visible light responsive Fe and N co-doped TiO2 nanoparticles. Ceram. Int. 43 (1), 973–981.

MacDonald, J.R., 1973. Theory of space-charge polarization and electrode-discharge effects. J. Chem. Phys. 58 (11), 4982–5001.

Mahanty, S., Roy, S., Sen, S., 2004. Effect of Sn doping on the structural and optical properties of sol–gel TiO2 thin films. J. Cryst. Growth 261 (1), 77–81.

Mofokeng, S., Kumar, V., Kroon, R., Ntwaeaborwa, O., 2017. Structure and optical properties of Dy3+ activated sol-gel ZnO-TiO2 nanocomposites. J. Alloy. Compd. 711, 121–131.

Nian, J.-N., Chen, S.-A., Tsai, C.-C., Teng, H., 2006. Structural feature and catalytic performance of Cu species distributed over TiO2 nanotubes. J. Phys. Chem. B 110 (51), 25817–25824.

Okada, K., Yamamoto, N., Kameshima, Y., Yasumori, A., MacKenzie, K.J., 2001. Effect of silica additive on the anatase-to-rutile phase transition. J. Am. Ceram. Soc. 84 (7), 1591–1596.

Okutan, M., Basaran, E., Bakan, H.I., Yakuphanoglu, F., 2005. AC conductivity and dielectric properties of Co-doped TiO2. Physica B 364 (1–4), 300–305.

Sen, S., Mahanty, S., Roy, S., Heintz, O., Bourgeois, S., Chaumont, D., 2005. Investigation on sol–gel synthesized Ag-doped TiO2 cermet thin films. Thin Solid Films 474 (1–2), 245–249.

Tripathy, S.K., Pattanaik, A., 2016. Optical and electronic properties of some semiconductors from energy gaps. Opt. Mater. 53, 123–133.

Tsai, S.-J., Cheng, S., 1997. Effect of TiO2 crystalline structure in photocatalytic degradation of phenolic contaminants. Catal. Today 33 (1–3), 227–237.

Wang, Y., Li, L., Huang, X., Li, Q., Li, G., 2015. New insights into fluorinated TiO 2 (brookite, anatase and rutile) nanoparticles as efficient photocatalytic redox catalysts. RSC Adv. 5 (43), 34302–34313.

Wang, K.-P., Teng, H., 2009. Zinc-doping in TiO 2 films to enhance electron transport in dye-sensitized solar cells under low-intensity illumination. PCCP 11 (41), 9489–9496.

Xu, H., Liu, Y., Xu, C., Liu, Y., Shao, C., Mu, R., 2006. Room-temperature ferromagnetism in (Mn, N)-codoped ZnO thin films prepared by reactive magnetron cosputtering. Appl. Phys. Lett. 88, (24) 242502.

Ye, J., Li, B., Li, M., Zheng, Y., Wu, S., Han, Y., 2020. ROS induced bactericidal activity of amorphous Zn-doped titanium oxide coatings and enhanced osseointegration in bacteria-infected rat tibias. Acta Biomater.

Yu, J.C., Lin, J., Kwok, R.W., 1998. Ti1-x Zr x O2 Solid Solutions for the Photocatalytic Degradation of Acetone in Air. J. Phys. Chem. B 102 (26), 5094–5098.

Yu, Y., Wang, J., Li, W., Zheng, W., Cao, Y., 2015. Doping mechanism of Zn 2+ ions in Zn-doped TiO 2 prepared by a sol–gel method. CrystEngComm 17 (27), 5074–5080.

Yu, J., Yu, X., Jul. 2008. Hydrothermal Synthesis and Photocatalytic Activity of Zinc Oxide Hollow Spheres. Environ. Sci. Technol. 42 (13), 4902–4907. https://doi.org/10.1021/es800036n.

Zhu, G., Cheng, Z., Lv, T., Pan, L., Zhao, Q., Sun, Z., 2010. Zn-doped nanocrystalline TiO 2 films for CdS quantum dot sensitized solar cells. Nanoscale 2 (7), 1229–1232.